Computational Multiscale Modeling of Pulsed Field Ablation Considering Conductivity and Damage Anisotropy Reveals Deep Lesion Morphologies

Quim Castellvi and Antoni Ivorra

Department of Engineering, Universitat Pompeu Fabra, Barcelona, Spain

Correspondence: Quim Castellvi (quim.castellvi@upf.edu), Antoni Ivorra (antoni.ivorra@upf.edu)

Keywords

Cardiac Ablation; Pulsed Field Ablation; PFA; Multiscale Modeling; Numerical Model; Mathematical Model; Anisotropy.

Funding

This project has received funding from the La Marató de TV3 foundation under the 202320-30 research project.

Conflicts of Interest

Dr. Castellvi is inventor of several patents pending and granted related to electroporation applications, has been a consultant of MedLumics SL and CardioFocus, Inc., and reports the equity ownership of Galvanize Therapeutics Inc. Dr. Ivorra has been a consultant for Argá Medtech SA, MedLumics SL, Boston Scientific and CardioFocus, Inc.

Data Availability

The data that support the findings of this study are available from the corresponding author upon reasonable request.

Ethics Statement

None

Abstract

Introduction

Pulsed Field Ablation (PFA) is an electroporation-based treatment modality to perform cardiac tissue ablations. Heart parenchyma is mainly constituted by elongated myocytes organized in fibers. This anisotropic morphology results in a preferential pathway for the electric current to flow along. Assuming conventional PFA modeling approaches in which lesions form where the electric field surpasses a threshold, such conductance anisotropy would result in relatively wide and shallow lesion morphologies when PFA applications are delivered with a focal monopolar catheter. Contrary to that, some recent preclinical data present narrow and deep elongated lesions. This study presents a multiscale simulation approach able to estimate electroporation treatments outcomes when applied in a high anisotropic tissue such as the myocardium.

Methodology

First, a microscopic model was implemented mimicking the conformation of the cardiac tissue. Longitudinal and transversal electric fields at different frequencies and magnitudes were applied to characterize the expected anisotropic behavior at tissue level in terms of electric conductivity and expected membrane disruption due to electroporation. Second, the microscopic characterization was integrated into a macroscopic model of a focal ablation catheter in contact with the myocardial tissue to simulate the delivery monopolar PFA treatments.

Results

The microscopic simulations results show that when low electric field magnitudes are applied, the induced membrane disruptions are predominantly appearing in fibers parallel to the electric field. However, at higher fields magnitudes, a demarcated superior sensitivity is observed in perpendicular orientation. The integration of these anisotropic properties into the macroscopic model predicts width/depth ratios of 1.2 compared to the ratios of about 2 predicted with the conventional modelling.

Conclusion

The multiscale model and approach presented here predicts relatively narrow and deep lesions as observed preclinically.

Introduction

Pulsed Field Ablation (PFA) is a groundbreaking nonthermal modality based on electroporation for cardiac ablation [1]. This technique uses very short electric pulses to generate high-intensity electric fields in target tissues. The electroporation phenomenon occurs when the large membrane voltage induced by the field, disrupts the cell membrane integrity by creating hydrophilic pores [2]. The increased permeability of the membrane can effectively result in the cell death while sparing the extracellular matrices of nearby structures such as nerves and blood vessels [3], [4]. Unlike thermal techniques, such as radiofrequency (RF) ablation or cryoablation, PFA minimizes collateral damage and reduces the risks associated with heat-related complications, making it an attractive option for treating cardiac arrhythmias [5], [6].

It is generally assumed that electroporation occurs in tissues where the electric field magnitude surpasses a threshold specific to both the tissue type and the applied waveform. And such assumption is effectively used to predict lesion morphologies in homogenous tissues by computing the electric field distribution [7], [8], [9], [10]. Cardiac tissue, however, presents unique challenges due to its highly anisotropic structure. The myocardium is composed of elongated myocytes arranged in fibers that are oriented predominantly perpendicular to the endocardial surface. This structural anisotropy introduces directional dependencies in electrical conductivity, with higher conductivity along the fiber orientation compared to the transverse direction. As observed in skeletal muscle [11], when PFA is applied at the myocardium the electric field is expected to distribute preferentially along the fibers [12], resulting in wider and shallower lesion morphologies than in isotropic tissues. Nevertheless, recent preclinical studies have reported relatively narrow and deep lesions when PFA is applied [13], [14], [15], [16], with lesion axes extending along a direction not strictly aligned with the expected current pathways dictated by fiber orientation. As also pointed by a recent study [17], this experimental data suggests the presence of additional factors influencing the electric and cell damage distribution that must be identified.

Understanding these discrepancies is crucial for optimizing PFA treatment parameters and improving its predictability and efficacy. Given the complexity of the myocardial structure and the dynamic interplay between electric field parameters, tissue conductivity, and cellular responses, a multiscale approach is essential to bridge the gap between cellular-level mechanisms and tissue-level outcomes. This type of multiscale models have been proven effective to link macroscopic phenomena to effects at microscopic scale [11], [18].

This study aims to investigate the factors driving the anisotropic behavior of lesion formation in cardiac tissue during PFA treatments. To achieve this, we employ a multiscale simulation framework combining microscopic and macroscopic modeling. At the cellular level, multiple simulations are carried out to evaluate the interactions between electric fields, ionic currents, and cell membranes under different conditions of electric field intensity, frequency, and cell orientations. These cellular-scale behaviors are incorporated into a macroscopic model to simulate, at tissue level, a focal PFA ablation in the heart. By integrating these scales, this study seeks to uncover the mechanisms behind the anisotropic lesion shapes observed during PFA and provide a robust framework for improving predictive tools and guiding clinical practice.

Materials and Methods

The multilevel approach consists of two computational models: one to explore the microscopic behavior of the parenchyma under external electric fields, and another one of macroscopic scale to incorporate that behavior and determine the therapeutic outcomes of the PFA treatment.

The first objective of the microscopic model is to evaluate the conductivity of the myocardium at the desired PFA frequency waveform, electric field magnitude, and cell orientation. These values are later used at tissue level to establish the parallel and perpendicular conductivities according to the macroscopic fiber directions. A second key role of microscopic model is to calculate the expected induced membrane voltage and altered membrane properties due to electroporation. The correlation between the applied electric field and the membrane permeabilization is employed by the macroscopic model to determine the lesion extension.

Both microscopic and macroscopic models were built and solved using the Finite Element Method provided by COMSOL Multiphysics 6.0 (Comsol Inc., Sweden) with its AC/DC module.

Microscopic Parenchyma Model

Geometric Mode

Cardiac cells possess a characteristic elongated rod-like shape. In multiple microscopic simulations studies, a cylinder has been employed to represent the myocyte geometry [19], [20]. This study uses the same approach to represent the myocytes as a cylinders of 100 µm length and 22 µm diameter (Figure 1a), based on cardiomyocyte morphology [21]. To avoid nanoscale geometric elements, the membrane of each cell has been represented as a surface with electrical properties equivalent to a 5 nm thickness membrane [22].

The transversal distribution of the myocytes has been generated using a hexagonal shape (Figure 1b) where, at physiological state, the extracellular volume accounts for a 22% of the total volume [23].

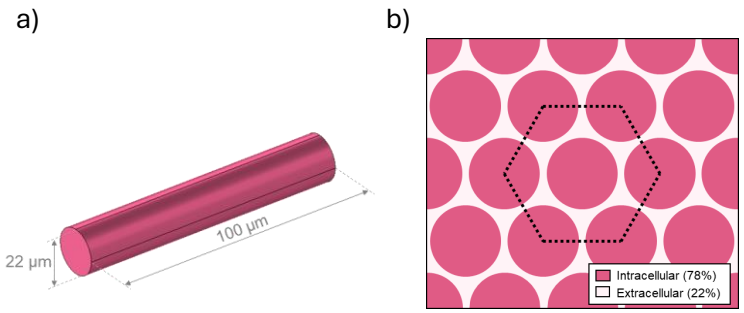

Figure 1 – Representation of the geometric distribution of cylindric representation of myocytes in the parenchyma model. a) Cylindric representation of a myocyte employed in the model. b) Hexagonal distribution according to the intracellular and extracellular ratio.

In order to generate an intercalated structure mimicking the complex interconnections between cardiomyocytes along the same fiber, each cell has been dislocated transversally to minimize the unrealistic straight paths extracellular medium and to allow lateral connectivity between the cardiomyocyte lines (Figure 2a). From the structure, two orthogonal directions can be defined longitudinal and transversal to the cardiomyocyte fibers (Figure 2b).

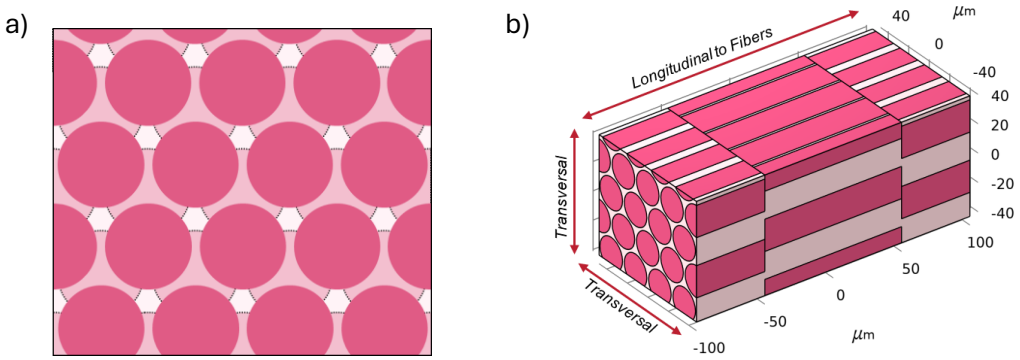

Figure 2 - a) Displacement between layers of myocytes fibers. b) Tridimensional representation of the geometrical model employed to calculate the microscopic environment of the cardiac tissue. Fiber direction determines the indicated transversal and longitudinal tissue directions.

Electrical Properties

The electrical properties of the different elements of the microscopic model can be found on Table 1.

Table 1 – Electrical properties of the microscopic model.

Property	**Value**	**Reference**
Extracellular conductivity (σ_e)	$1.5\ S/m$	[24]
Extracellular relative permittivity (ϵ_e)	70	[24]
Intracellular conductivity (σ_i)	$0.5\ S/m$	[24]
Intracellular relative permittivity (ϵ_i)	70	[24]
Membrane conductivity (σ_{m0})	$2.5 \times 10^{-7}\ S/m$	[24]
Membrane relative permittivity (ϵ_m)	5	[24]
Membrane pore conductivity (σ_{pore})	$0.9\ S/m$	[25]

Boundary conditions

The static membrane conductivity (σ_m) dependence to the electroporation phenomenon has been modeled as an exponential function, see equation (1), as previously described [24]. The transmembrane voltage (V_m) has been calculated as the voltage difference between sides of the defined surfaces.

$$\sigma_m = \sigma_{m0} + 0.7\ S/m \cdot \left(\frac{V_m}{1\ V}\right)^{12} \quad (1)$$

The specific electric field distribution and the resulting electric conductivity of the parenchyma has been studied in two different directions with respect to the fiber orientation. In order to generate the electric field magnitude ($|E|$) at the desired direction, a differential potential was defined between two opposite external surfaces of the microscopic model (see Figure 3). The remaining opposite surfaces pairs were considered to have a periodical condition to preserve the repetitive microstructure structure of the parenchyma.

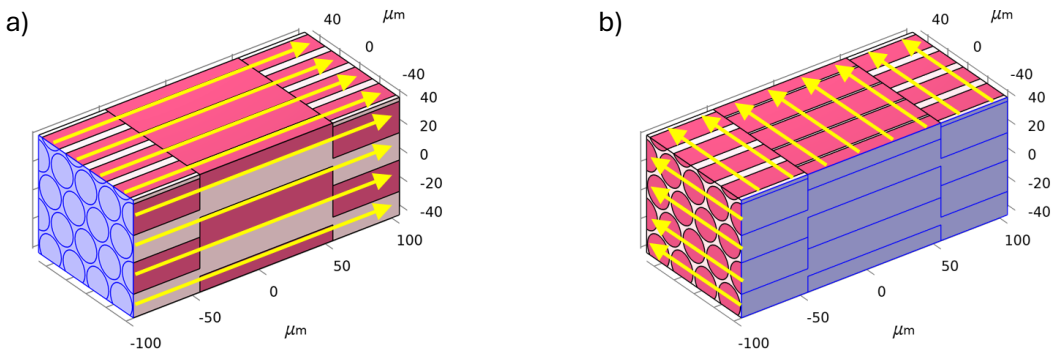

Figure 3 - Representation of the microscopic model with the iso-potential surfaces (blue) and representation of the electric field (yellow arrows) applied: a) Longitudinal to the fibers b) Transversal to the fibers.

Considering the symmetry of the defined microscopic geometry of the myocardium, a model composed of 32 cells (4x4x2) was finally employed to conduct the results with a reduced computational cost.

Damage Assessment

The cellular damage has been linked to relative pore area (RPA) induced by the electroporation pulses [25]. Since the relative are of pores can be derived from the cell surface conductance (G_s) as denoted in (2), the has been extracted by integrating the membrane conductivity over the membrane surface (S_m) of the most central cell of the model (Figure 4) (see equation (3)).

$$RPA = \frac{G_s}{\sigma_{pore} \cdot S_m} \tag{2}$$

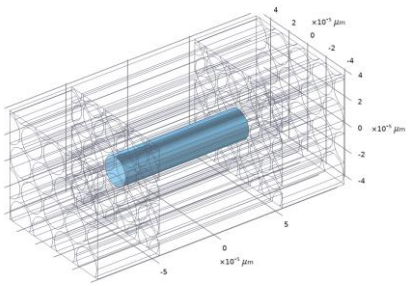

Figure 4 - Identification of the representative cell employed to calculate the membrane damage.

$$G_s = \oiint \sigma_m \, dS_m \tag{3}$$

Using this simplified approach, the dependence between RPA and electric field can be captured in functions for transversal (RPA_T) and longitudinal (RPA_L) directions.

In electroporation-based treatments, for a specific tissue and for a specific pulse waveform, a single macroscopic electric field magnitude has been traditionally employed as the threshold for predicting the affected areas. However, considering the anisotropy between transverse and longitudinal directions observed in the microscopic simulations, for a specific value of RPA required to induce a lethal IRE outcome, the electric field required can be highly dependent to the fiber orientation.

Macroscopic Therapeutic Model

Geometric Mode

Following the simplified model for monopolar applications in PFA previously reported [26], a 3D model observed in Figure 5 was defined.

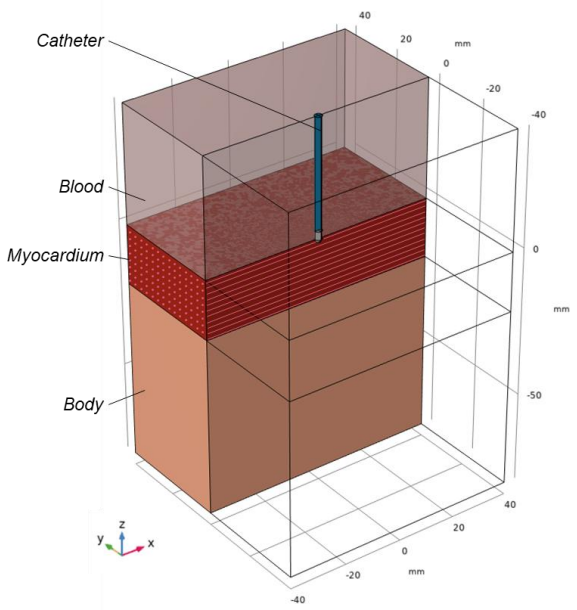

Figure 5 - 3D geometric model of a monopolar PFA application with an 8Fr focal ablation catheter immersed in blood is in contact to the myocardium with fibers oriented on the x axis parallel to the endocardium.

A geometric cube of 40 mm is split between blood and myocardium domains. A 7F catheter (2.33 mm) diameter was positioned perpendicular to the myocardium with 1.25 mm of indentation into the parenchyma to simulate a medium contact force [27].

Electrical Properties

The constant electrical properties of the different materials are defined in Table 2. It must be noticed that the in-silico setup is aiming to simulate illustratively a PFA treatment using 100 kHz biphasic waveform, thus the properties of the tissue have been selected accordingly.

Table 2 – Electrical properties of the macroscopic model.

Property	Value	Reference
Blood Conductivity	$0.7\ S/m$	[28]
Isolator Conductivity	$1 \times 10^{-5}\ S/m$	[29]
Electrode Conductivity	$4.6 \times 10^{6}\ S/m$	[29]

The myocardial conductivity at the different electric fields and at the specific frequency of 100 kHz has been obtained by linear interpolation using the microscopic model results. Values for myocardium conductivity for longitudinal (σ_L) and transversal (σ_T) directions can be observed in Figure 6.

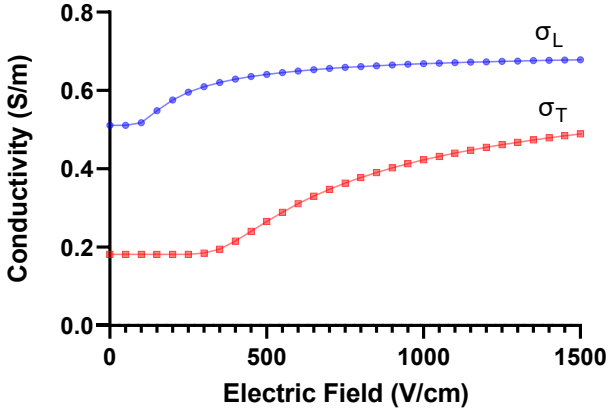

Figure 6 - Electric conductivity of myocardium at different electric field intensities for a 100 kHz PFA waveform.

The model defines the myocardium fiber being all oriented along the x-axis and parallel to the endocardial surface. Accordingly, the electrical conductivity was defined as a diagonal tensor shown in equation (4).

$$\sigma_{myo} = \begin{bmatrix} \sigma_L(|E|) & 0 & 0 \\ 0 & \sigma_T(|E|) & 0 \\ 0 & 0 & \sigma_T(|E|) \end{bmatrix} \quad (4)$$

Boundary Conditions

The distal tip of the focal catheter has been arbitrary defined with a total current of 10 A flowing towards the dispersive electrode ($\varphi = 0\ V$) placed at the bottom of the model. Electric insulation has been defined for the remaining outer surfaces of the model.

Damage Assessment

The level of permeabilization at the different electric field magnitudes and orientations obtained in the microscopic simulations (RPA_L and RPA_T) have been used to capture the anisotropic electroporation sensitivity to fields oriented longitudinal and transversal to the fibers. As an aproximation, the total degree of permeabilization has been calculated as the magnitude of the RPA vector obtained from the electric field compound as denoted in equation (5).

$$RPA = \sqrt{RPA_L(|E_x|)^2 + RPA_T\left(|E_y|\right)^2 + RPA_T(|E_z|)^2} \quad (5)$$

Results

Microscopic Parenchyma Model

Using the microstructure model the impedance values at frequencies from 1 kHz to 10 MHz were assessed under non-electroporation conditions (0.1 V/cm applied). Figure 7 shows the expected conductivity at the different assessed frequencies.

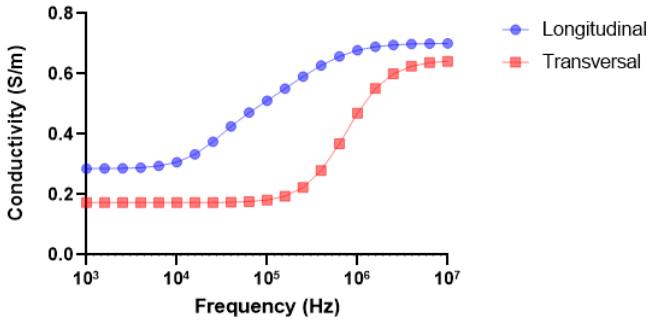

Figure 7 – Low field (0.1 V/cm) longitudinal and transversal electric conductivity at the different assessed frequencies using the microscopic model.

The obtained results show conductivities at 1 kHz of 0.17 S/m transversally and 0.29 S/m longitudinally to the fibers. These values agree with the [0.14 S/m– 0.18 S/m] transversal and longitudinal [0.40 S/m – 0.47 S/m] measured experimentally [30], [31]. At higher frequencies (10 MHz), the difference between perpendicular (0.64 S/m) and parallel (0.70 S/m) orientations are less demarcated, and in agreement to the 0.68 S/m experimentally measured agnostically to fiber orientation [32].

The parenchyma conductivity has been also assessed at additional electric field magnitudes up to 3000 V/cm for which the electroporation phenomenon is present. Figure 8 presents a representative change of conductivity at the different frequencies when electroporation magnitudes are reached on the parenchyma.

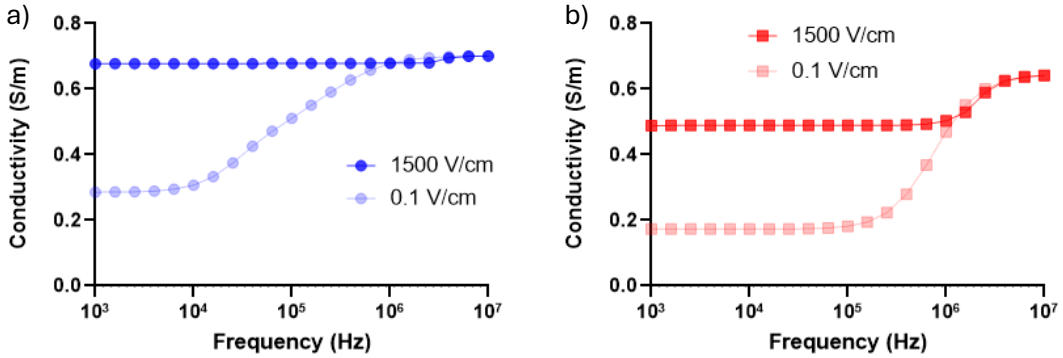

Figure 8 - Electric conductivity of myocardium at different frequencies when non-electroporation (E = 0.1 V/cm) and electroporation phenomenon is present (E = 1500 V/cm. a) Electric field applied longitudinally to the fibers. b) Electric field applied transversely to fibers.

The expected myocardium electric properties for specific pulse waveform frequencies have been assessed at the different electric fields. Illustrative results can be observed in Figure 9 for frequencies of 10 kHz, 100 kHz and 1 MHz.

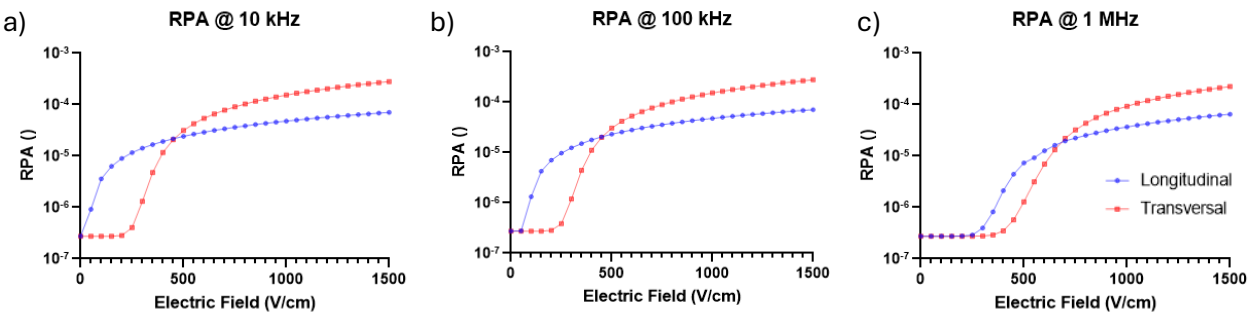

Figure 9 - Relative Pore Area (RPA) at the different electric field magnitudes for a PFA waveform frequency of: a) at 10 kHz, b) at 100 kHz and c) at 1 MHz.

Macroscopic Therapeutic Model

A PFA treatment using 10 A at 100 kHz has been considered as an illustrative simulation. The model predicts a voltage of 1182 V at the catheter tip resulting in a 118 Ω load. This can be considered within the range of the typical expected impedance at this high frequency range [33].

The results in this section are presented visualizing the transversal cut plane parallel to the fiber orientation and perpendicular to the myocardium. Figure 10a shows the electric field distribution.

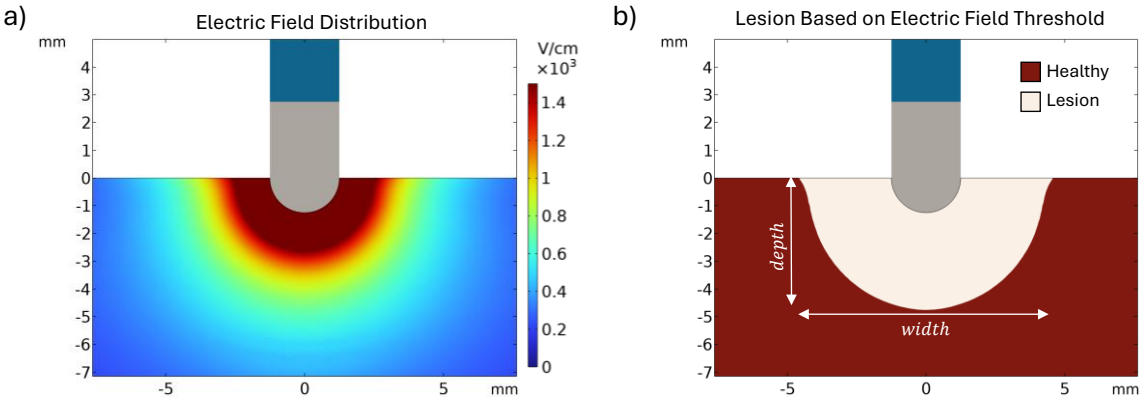

Figure 10 – Results from the macroscopic simulation when 10 A are applied at the tip of the catheter in a monopolar fashion. a) Electric field distribution with color scale limited to 1.5 kV/cm for visualization. b) Predicted lesion extension when 700 V/cm are employed as lethal threshold.

A previous in-vivo study reported a lethal electric field threshold between 600 V/cm and 800 V/cm when a pulses at 90 kHz were employed [34]. In the present study, 700 V/cm has been considered as the lethal electric field threshold for the myocardium using a waveform of 100 kHz. Figure 10b shows the lesion shape with a resulting width of 9.2 mm and a depth of 4.8 mm. These dimensions result in a (width/depth) lesion shape ratio of 1.92, substantially larger than some reported during preclinical studies [13], [14], [15], [16].

For that specific pulse protocol, the tissue at 4.8 mm depth just under the electrode are subject to a pure perpendicular field of 700 V/cm. According to the microscopic simulations (Figure 9b), for a transversal cell, this would result in a lethal RPA threshold of 5.5×10^{-5}. Since RPA represents the ratio of damaged membrane, it can be linked to the cell's limits to resist the resulting homeostatic loss.

Based on the electric field magnitude and fiber orientation, Figure 11a shows the expected RPA distribution.

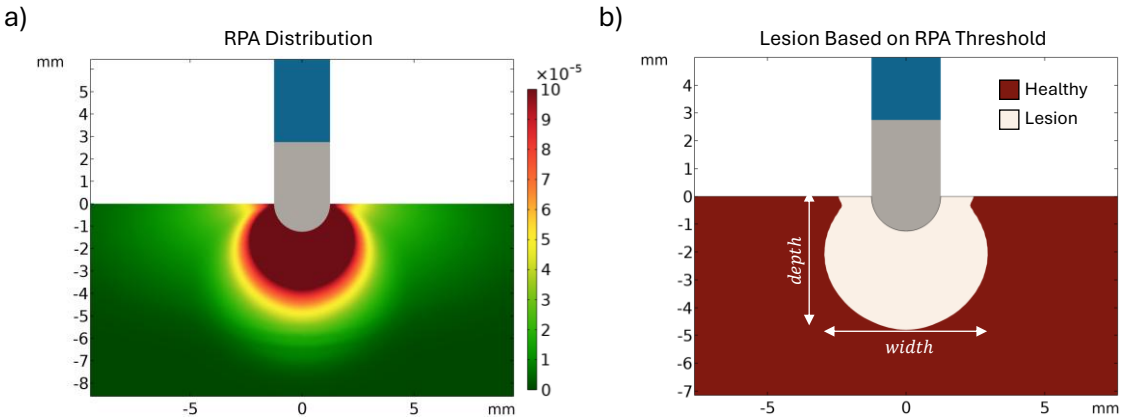

Figure 11 – Results from the macroscopic simulation when 10 A are applied at the tip of the catheter in a monopolar fashion. a) RPA distribution with color scale limited to 10×10^{-5} for visualization. b) Predicted lesion extension when 5.5×10^{-5} is employed as lethal RPA threshold and the anisotropic sensitivity with the fiber orientation is considered.

When the lethal threshold is defined, Figure 11b presents the expected lesion shape. Observing the lesion parallel to the fibers, the results predict a lesion depth of 4.8 mm, but with an expected width of 5.9 mm. This substantial reduction in lesion width results in a lesion shape ratio of 1.23, a closer value to the reported experimental data.

Figure 12 compares the lesion shape between a conventional model based on the electric field with a model presented here based on the RPA which includes the damage anisotropy of the myocardium to the electric field magnitude. This figure presents both perpendicular and parellel cut to the fiber direction to illustrate the variation expected at different planes of evaluation.

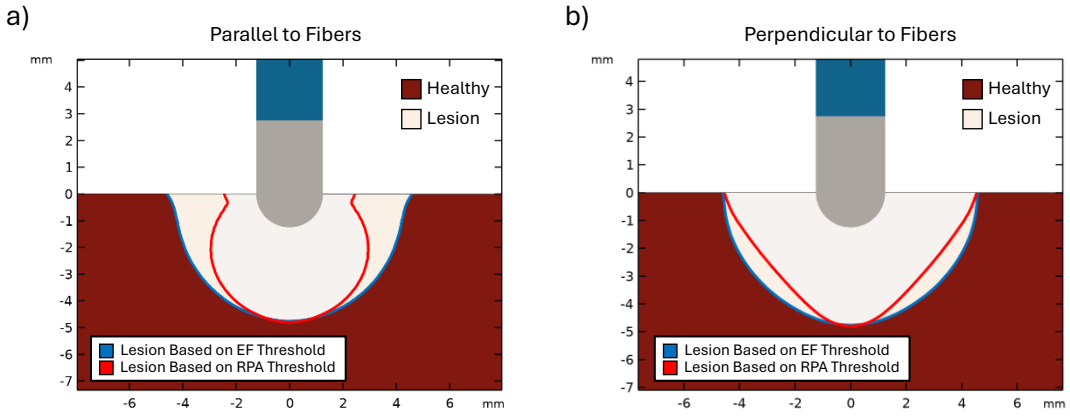

Figure 12 - Predicted lesions extension: With a conventional model based on the electric field (EF) threshold (blue line perimeter). With a model based on the RPA threshold and including the damage anisotropy of myocardium to the electric field magnitude (red line perimeter). a) In a perpendicular cut to the fiber direction. b) In a parallel cut to the fiber direction.

Even presenting the same lesion depth, the volume without the damage sensitivity shows a value of 93.8 mm^3 whereas when anisotropic effects are considered the expected lesion volume drops to 55.4 mm^3.

Discussion

The proposed multiscale modeling allowed us to explore the expected electroporation effect at cellular level and to incorporate such effects within a macroscopic model of the sort commonly used to predict the therapeutic outcomes of PFA.

The microscopic simulations denote that for low electric field magnitudes, fibers parallel to the electric field are going to be the single ones affected by the pulses. This higher electroporation sensitivity of the longitudinal fibers at lower electric fields was previously reported in skeletal muscle [35]. However, the percentage of membrane able to be damaged in a longitudinal direction makes it difficult to reach the required lethal damage.

On the other hand, when electric field is applied perpendicular to the myocytes, the required electric field to induce electroporation is much larger due to the small cell diameter. However, once the electric field is large enough, a large fraction of the myocyte is exposed to the electroporation phenomenon resulting in a rapid increase in membrane damage.

As can be observed in Figure 9, the selection of the frequency will have an impact on the sensitivity of both transversal and longitudinal fibers to the electric field. According to this, the selection of the pulse protocol in terms of frequency, repetition and magnitude will have not only an impact on the extension of the lesion but also the induced lesion shape. Being able to predict and manipulate this shape dependence could play a key role in the development and expansion of PFA technology in the clinical field.

Study Limitations

The hypothesis and findings presented here can help to understand the unexpected lesion shapes observed during preclinical studies. Although employing a multiscale model is sufficient to elucidate the plausibility of the hypothesis, the model presents several limitations that should be considered for future research.

The geometric representation of the cells and its organization has been employed to minimize the computational cost and clarity of the results. However, more realistic geometries and intracellular content can be relevant for further analysis, particularly in case of nsPEF where intracellular structures can be also be affected by electroporation [36], [37].

Another important aspect to consider is the potential role that gap junctions can play. The presence of low conductivity paths between contiguous longitudinal cells can not only affect the impedance of the parenchyma but the ability to build-up membrane voltage during the electric pulses. This can bring resilience to the intercalated discs of the myocardium, thus, the longitudinal sensitivity of the parenchyma to PFA.

Although a highly complex model exists to model the dynamic aperture of the pores during the application of the pulse [38], [39], a static simplification has been employed. This function has been proven as effective to explain experimental results observed in-vitro [40] as well as requiring a lower computational complexity of the simulations. Nevertheless, incorporating a dynamic model of pore formation may elucidate additional mechanisms and specific features of electroporation in anisotropic tissues.

Regarding the macroscopic model, it must be noticed that all the fibers were defined as completely parallel to the epicardial surface. This simplistic orientation differs substantially from reality, where orientation at the endocardium and endocardium is closer to the perpendicular [41] and transitions to parallel at the inner areas of the cardiac wall [42]. In addition parallel cuts have been considered for evaluation in this study. Overall, this could lead to a large experimental variability of lesion shapes even using the same pulse parameter and therapeutic setup.

Conclusions

This study indicates that the narrow and deep lesion shape observed in focal unipolar treatments can be at least partially explained not only by the electrical conductivity anisotropy of the myocardium but also by its anisotropy in terms of damage by electroporation. The multiscale model approach estimates similar shape ratios to the ones observed experimentally. The multiscale approach presented here has been successfully employed to anticipate the anisotropic behavior of the myocardium during the PFA treatments. Although the model requires further experimental valiedation, it could improve the current predictive tools, the understanding of the technology and potentially improving the future PFA clinical outcomes.

Ethics Statement

None

References

[1] A. Verma, S. J. Asivatham, T. Deneke, Q. Castellvi, and R. E. Neal, "Primer on Pulsed Electrical Field Ablation: Understanding the Benefits and Limitations," *Circ. Arrhythmia Electrophysiol.*, vol. 14, no. 9, p. E010086, 2021, doi: 10.1161/CIRCEP.121.010086.

[2] L. Delemotte and M. Tarek, "Molecular dynamics simulations of lipid membrane electroporation," *J. Membr. Biol.*, vol. 245, no. 9, pp. 531–543, 2012, doi: 10.1007/s00232-012-9434-6.

[3] J. Koruth *et al.*, "Preclinical Evaluation of Pulsed Field Ablation: Electrophysiological and Histological Assessment of Thoracic Vein Isolation," *Circ. Arrhythmia Electrophysiol.*, vol. 12, no. 12, pp. 1–9, 2019, doi: 10.1161/CIRCEP.119.007781.

[4] E. Maor, A. Ivorra, J. Leor, and B. Rubinsky, "The effect of irreversible electroporation on blood vessels," *Technol. Cancer Res. Treat.*, vol. 6, no. 4, pp. 307–312, 2007, doi: 10.1177/153303460700600407.

[5] E. Ekanem *et al.*, "Safety of pulsed field ablation in more than 17,000 patients with atrial fibrillation in the MANIFEST-17K study," *Nat. Med.*, vol. 30, no. 7, pp. 2020–2029, 2024, doi: 10.1038/s41591-024-03114-3.

[6] D. G. Della Rocca *et al.*, "Pulsed electric field, cryoballoon, and radiofrequency for paroxysmal atrial fibrillation ablation: A propensity score-matched comparison," *Europace*, vol. 26, no. 1, pp. 1–10, 2024, doi: 10.1093/europace/euae016.

[7] N. Pavšelj and D. Miklavčič, "Numerical modeling in electroporation-based biomedical applications," *Radiol. Oncol.*, vol. 42, no. 3, pp. 159–168, 2008, doi: 10.2478/v10019-008-0008-2.

[8] D. Miklavčič, K. Beravs, D. Šemrov, M. Čemažar, F. Demšar, and G. Serša, “The importance of electric field distribution for effective in vivo electroporation of tissues,” *Biophys. J.*, vol. 74, no. 5, pp. 2152–2158, 1998, doi: 10.1016/S0006-3495(98)77924-X.

[9] S. Corovic, I. Lackovic, P. Sustaric, T. Sustar, T. Rodic, and D. Miklavcic, “Modeling of electric field distribution in tissues during electroporation,” *Biomed. Eng. Online*, vol. 12, no. 1, pp. 1–27, 2013, doi: 10.1186/1475-925X-12-16.

[10] R. E. Neal *et al.*, “In vivo irreversible electroporation kidney ablation: Experimentally correlated numerical models,” *IEEE Trans. Biomed. Eng.*, vol. 62, no. 2, pp. 561–569, 2015, doi: 10.1109/TBME.2014.2360374.

[11] R. Smerc *et al.*, “A Multiscale Computational Model of Skeletal Muscle Electroporation Validated Using In Situ Porcine Experiments,” *IEEE Trans. Biomed. Eng.*, vol. 70, no. 6, pp. 1826–1837, 2023, doi: 10.1109/TBME.2022.3229560.

[12] F. Xie and C. W. Zemlin, “Effect of twisted fiber anisotropy in cardiac tissue on ablation with pulsed electric fields,” *PLoS One*, vol. 11, no. 4, pp. 1–21, 2016, doi: 10.1371/journal.pone.0152262.

[13] A. Verma *et al.*, “Characteristics of Pulsed Electric Field Cardiac Ablation Porcine Treatment Zones with a Focal Catheter,” *J. Cardiovasc. Electrophysiol.*, vol. 0, no. 0, pp. 0–2, Nov. 2022, doi: 10.1111/jce.15734.

[14] H. Nakagawa *et al.*, “Effects of Contact Force on Lesion Size During Pulsed Field Catheter Ablation: Histochemical Characterization of Ventricular Lesion Boundaries,” *Circ. Arrhythmia Electrophysiol.*, vol. 17, no. 1, pp. 11–23, 2024, doi: 10.1161/CIRCEP.123.012026.

[15] M. Emami *et al.*, “Ca-527-04 Association Between Lesion Size and Field Strength of Pulsed Field Ablation,” *Hear. Rhythm*, vol. 19, no. 5, p. S4, 2022, doi: 10.1016/j.hrthm.2022.03.094.

[16] G. Amorós-Figueras, S. Casabella-Ramon, Z. Moreno-Weidmann, A. Ivorra, J. M. Guerra, and T. García-Sánchez, “Dynamics of High-Density Unipolar Epicardial Electrograms During PFA,” *Circ. Arrhythmia Electrophysiol.*, vol. 16, no. 9, p. E011914, 2023, doi: 10.1161/CIRCEP.123.011914.

[17] A. Petras *et al.*, “The use of a single electric field lethal threshold for PFA lesion prediction is not sufficient to characterize the lesion dimensions Matches lesion width na l P re r f,” *Hear. Rhythm O2*, 2025, doi: 10.1016/j.hroo.2025.02.014.

[18] S. Huclova and J. Fröhlich, “Towards a realistic dielectric tissue model: A multiscale approach,” *2010 Annu. Int. Conf. IEEE Eng. Med. Biol. Soc. EMBC’10*, pp. 6813–6816, 2010, doi: 10.1109/IEMBS.2010.5625963.

[19] P. Haftbaradaran Esfahani, J. Westergren, L. Lindfors, and R. Knöll, “Frequency-dependent signaling in cardiac myocytes,” *Front. Physiol.*, vol. 13, no. September, pp. 1–12, 2022, doi: 10.3389/fphys.2022.926422.

[20] A. Tveito, K. H. Jæger, M. Kuchta, K. A. Mardal, and M. E. Rognes, “A cell-based framework for numerical modeling of electrical conduction in cardiac tissue,” *Front. Phys.*, vol. 5, no. OCT, pp. 1–18, 2017, doi: 10.3389/fphy.2017.00048.

[21] R. E. Tracy and G. E. Sander, “Histologically measured cardiomyocyte hypertrophy correlates with body height as strongly as with body mass index,” *Cardiol. Res. Pract.*, vol. 1, no. 1, 2011, doi: 10.4061/2011/658958.

[22] R. W. Glaser, S. L. Leikin, L. V. Chernomordik, V. F. Pastushenko, and A. I. Sokirko, "Reversible electrical breakdown of lipid bilayers: formation and evolution of pores," *BBA - Biomembr.*, vol. 940, no. 2, pp. 275–287, 1988, doi: 10.1016/0005-2736(88)90202-7.

[23] R. Emig *et al.*, "Passive myocardial mechanical properties: meaning, measurement, models," *Biophys. Rev.*, vol. 13, no. 5, pp. 587–610, 2021, doi: 10.1007/s12551-021-00838-1.

[24] A. Ivorra, J. Villemejane, and L. M. Mir, "Electrical modeling of the influence of medium conductivity on electroporation," *Phys. Chem. Chem. Phys.*, vol. 12, no. 34, p. 10055, 2010, doi: 10.1039/c004419a.

[25] B. Mercadal, P. T. Vernier, and A. Ivorra, "Dependence of Electroporation Detection Threshold on Cell Radius: An Explanation to Observations Non Compatible with Schwan's Equation Model," *J. Membr. Biol.*, vol. 249, no. 5, pp. 663–676, 2016, doi: 10.1007/s00232-016-9907-0.

[26] M. Gómez-Barea, T. García-Sánchez, and A. Ivorra, "A computational comparison of radiofrequency and pulsed field ablation in terms of lesion morphology in the cardiac chamber," *Sci. Rep.*, vol. 12, no. 1, p. 16144, Sep. 2022, doi: 10.1038/s41598-022-20212-9.

[27] D. Schutt, E. J. Berjano, and D. Haemmerich, "Effect of electrode thermal conductivity in cardiac radiofrequency catheter ablation: A computational modeling study," *Int. J. Hyperth.*, vol. 25, no. 2, pp. 99–107, 2009, doi: 10.1080/02656730802563051.

[28] P. A. Hasgall *et al.*, "Tissue Properties Database V4.1," IT'IS Database for Thermal and Electromagnetic Parameters of Biological Tissues, Version 4.1. Accessed: Feb. 22, 2022. [Online]. Available: https://itis.swiss/virtual-population/tissue-properties/database/dielectric-properties.

[29] A. Gonzalez-Suarez and E. Berjano, "Comparative Analysis of Different Methods of Modeling the Thermal Effect of Circulating Blood Flow During RF Cardiac Ablation," *IEEE Trans. Biomed. Eng.*, vol. 63, no. 2, pp. 250–259, Feb. 2016, doi: 10.1109/TBME.2015.2451178.

[30] S. Rush, J. A. Abildskov, and R. McFee, "Resistivity of Body Tissues at Low Frequencies," *Circ. Res.*, vol. 12, no. 1, pp. 40–50, Jan. 1963, doi: 10.1161/01.RES.12.1.40.

[31] D. E. Roberts and A. M. Scher, "Effect of tissue anisotropy on extracellular potential fields in canine myocardium in situ," *Circ. Res.*, vol. 50, no. 3, pp. 342–351, 1982, doi: 10.1161/01.RES.50.3.342.

[32] A. Surowiec, S. S. Stuchly, L. Eidus, and A. Swarup, "In vitro dielectric properties of human tissues at radiofrequencies," *Phys. Med. Biol.*, vol. 32, no. 5, pp. 615–621, 1987, doi: 10.1088/0031-9155/32/5/007.

[33] A. Shapira-Daniels *et al.*, "Modulating the Baseline Impedance: An Adjunctive Technique for Maximizing Radiofrequency Lesion Dimensions in Deep and Intramural Ventricular Substrate," *Circ. Arrhythmia Electrophysiol.*, vol. 12, no. 6, pp. 1–12, 2019, doi: 10.1161/CIRCEP.119.007336.

[34] T. García-Sánchez *et al.*, "Parametric Study of Pulsed Field Ablation With Biphasic Waveforms in an In Vivo Heart Model: The Role of Frequency," *Circ. Arrhythmia Electrophysiol.*, vol. 15, no. 10, pp. 693–705, 2022, doi: 10.1161/CIRCEP.122.010992.

[35] S. Čorović *et al.*, “The influence of skeletal muscle anisotropy on electroporation: In vivo study and numerical modeling,” *Med. Biol. Eng. Comput.*, vol. 48, no. 7, pp. 637–648, 2010, doi: 10.1007/s11517-010-0614-1.

[36] A. Rossi *et al.*, “Nanosecond pulsed electric fields induce endoplasmic reticulum stress accompanied by immunogenic cell death in murine models of lymphoma and colorectal cancer,” *Cancers (Basel).*, vol. 11, no. 12, 2019, doi: 10.3390/cancers11122034.

[37] P. Thomas Vernier, A. Li, L. Marcu, C. M. Craft, and M. A. Gundersen, “Ultrashort Pulsed Electric Fields Induce Membrane Phospholipid Translocation and Caspase Activation: Differential Sensitivities of Jurkat T Lymphoblasts and Rat Glioma C6 Cells,” *IEEE Trans. Dielectr. Electr. Insul.*, vol. 10, no. 5, pp. 795–809, 2003, doi: 10.1109/TDEI.2003.1237329.

[38] W. Krassowska and P. D. Filev, “Modeling Electroporation in a Single Cell,” *Biophys. J.*, vol. 92, no. 2, pp. 404–417, Jan. 2007, doi: 10.1529/biophysj.106.094235.

[39] T. Kotnik, L. Rems, M. Tarek, and D. Miklavcic, “Membrane Electroporation and Electropermeabilization: Mechanisms and Models,” *Annu. Rev. Biophys.*, vol. 48, pp. 63–91, 2019, doi: 10.1146/annurev-biophys-052118-115451.

[40] K. Kinosita and T. Y. Tsong, “Voltage-induced conductance in human erythrocyte membranes,” *BBA - Biomembr.*, vol. 554, no. 2, pp. 479–497, 1979, doi: 10.1016/0005-2736(79)90386-9.

[41] J. Wong and E. Kuhl, “Generating fibre orientation maps in human heart models using Poisson interpolation,” *Comput. Methods Biomech. Biomed. Engin.*, vol. 17, no. 11, pp. 1217–1226, Aug. 2014, doi: 10.1080/10255842.2012.739167.

[42] R. Doste *et al.*, “A rule-based method to model myocardial fiber orientation in cardiac biventricular geometries with outflow tracts,” *Int. j. numer. method. biomed. eng.*, vol. 35, no. 4, pp. 1–17, 2019, doi: 10.1002/cnm.3185.